14th Australasian Fluid Mechanics Conference
Adelaide University, Adelaide, Australia
10-14 December 2001

Phase Averaged Velocity Field Within a Fluidic Precessing Jet Nozzle

C. Y. Wong[1], P. V. Lanspeary[1], G. J. Nathan[1], R. M. Kelso[1] and T. O'Doherty[2]

[1]Department of Mechanical Engineering
University of Adelaide, Adelaide, South Australia, 5005 AUSTRALIA
[2]School of Engineering, Division of Mechanical Engineering
University of Wales, Cardiff, Wales, United Kingdom, CF24 OYF

Abstract

A nozzle consisting of a round inlet orifice expanding suddenly into a short axisymmetric chamber is the basis of an industrial burner which produces lower levels of NO_x pollution than other, more conventional burners. The jet flow from the inlet orifice reattaches asymmetrically and precesses around the wall of the chamber. Phase-averaged measurements of axial velocity component in the chamber have shown that the length of the potential core of the inlet flow is about half that of an unconfined turbulent jet and the velocity decay rate is about twice as large. Entrainment by the reattaching flow induces a reverse flow in the nozzle. The measurements indicate that this reverse flow has a speed in the order of 30% of the forward flow speed. Work by other researchers on the effect of counter-flow on jets suggests that interaction between the reverse flow and the reattaching forward flow is largely responsible for the high spreading and decay rates of the latter.

Introduction

The Fluidic Precessing Jet (FPJ) nozzle (Figure 1) consists of a cylindrical chamber with a small axisymmetric inlet at one end and an exit lip at the other. The inlet flow separates at the abrupt inlet expansion and reattaches asymmetrically to the wall of the chamber [8]. The reattaching flow from the inlet precesses around the inside wall of the chamber and thus produces a precessing exit flow. The lip and large transverse pressure gradients near the outlet together steer the exit flow through a large angle, towards the axis and across the face of the nozzle outlet.

In the cement and lime industries, the FPJ nozzle has demonstrated significant reduction in NO_x emissions and improvement in product quality [4, 3]. These benefits are a result of differences between the combustion in the flow field of traditional axial-jet burners and the combustion produced by the FPJ [9] — which in turn depends on the differences in the turbulent-jet flow field.

Since the discovery of the FPJ by Nathan [7] and its first application as an industrial burner, a significant research effort has been directed at optimising the geometry of the FPJ nozzle and at understanding the FPJ flow. The early research on the FPJ consisted of flow visualisation studies, combustion trials and experiments with pressure transducers and uncalibrated hot-wire anemometers [7, 8, 6]. Newbold, Nathan, Nobes and Turns [10] have more recently confirmed that NO_x emissions from the FPJ are significantly lower than from conventional burners. Measurements of concentration scalar [11] and flow-field velocity [12] have confirmed the existence of very large scale, long-lived features in precessing-jet turbulence.

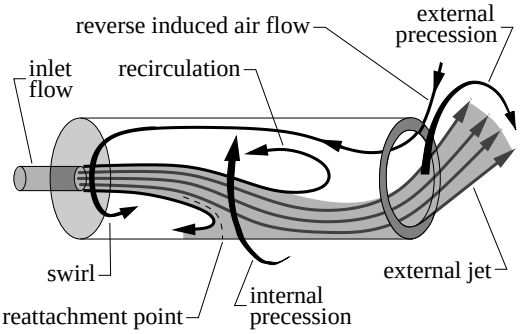

Figure 1: Quasi-2D representation of the internal FPJ flow field inferred from flow visualisation [7, 8].

Access to the flow inside an FPJ nozzle is restricted and the direction of the flow varies so much that the velocity field has not previously been measured. For example, extreme variations in the amplitude and direction of the velocity vector make meaningful hot-wire anemometry virtually impossible. This paper presents the first measurements of flow velocity within the precessing jet chamber. The measurements were obtained by laser-Doppler anemometry (LDA) and the signal from a pressure transducer was used as a reference for phase averaging of the LDA data.

Experimental Apparatus

The FPJ nozzle

The geometry and dimensions of the FPJ nozzle used for the measurements of the internal flow field are shown in Figure 2. The most important geometric parameters determining the behaviour of the flow are the inlet-diameter expansion ratio ($D/d = 5.07$), the length-to-diameter ratio of the chamber ($L/D = 2.7$) and the location and size of the centrebody. Nathan [7] observed that, in the absence of an obstruction just inside the exit plane, FPJ precession is intermittent, and that an obstruction such as the centrebody shown in Figure 2 improves the regularity and reliability of precession. The centrebody is supported on three radial struts, each with a diameter of 4.0 mm, and the exit lip has an upstream-facing chamfer of 45°.

Flow Conditioning

The air flow for the FPJ was obtained from an industrial air compressor via a pressure regulator, a 2000 l/min rotameter, a seeding ejector and, finally, a flow conditioner (Figure 3). The seeding ejector was supplied with sub-micron glycol particles from a "Rosco 4500" fog generator. Flow rates were determined from measurements of the flow speed 24 mm downstream from the FPJ inlet plane (Figure 4).

The flow conditioner provides a swirl-free, low-turbulence and

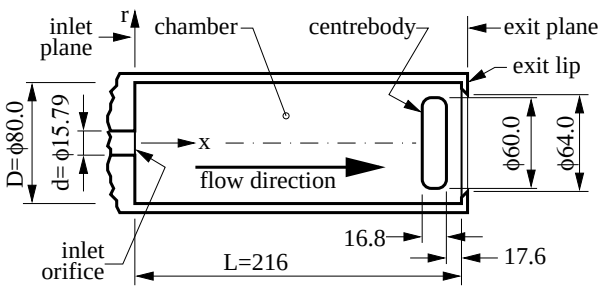

Figure 2: Dimensions and features of the FPJ nozzle used for LDA measurements of the internal flow field. Dimensions are in mm.

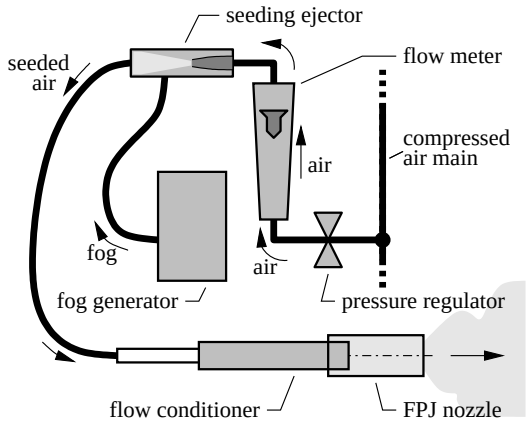

Figure 3: General arrangement of apparatus.

uniform flow at the FPJ inlet plane. It consists of a diffuser, a honeycomb section, a series of 5 screens and a contraction with a smooth profile. In order to avoid boundary-layer separation, the design of the diffuser follows the recommendations of Mehta [5]. The included angle of the diffuser is 9.1° and the area ratio is 2. The honeycomb has hexagonal cells with an equivalent length-to-diameter ratio of 11.0. The screens, which are constructed of 28 SWG wire woven at 16 MPI, help to reduce the intensity of large scale turbulence. Streamwise curvature, κ, of the wall is an important contributor to boundary-layer separation in contractions, and so, for local duct diameter d_l, the contraction profile is designed with the same maximum value of $|\kappa|/d_l$ in the concave region as in the convex region. The contraction, which has an area ratio of 10:1, further improves the uniformity and reduces the turbulence level of the flow.

At an inlet Reynolds number of $Re = U_i d/\nu = 43,000$, where U_i is the inlet flow speed and ν is the kinematic viscosity of air, the mean velocity distribution at the contraction outlet is very close to the ideal "top-hat" profile. The non-uniformity of the time-averaged air speed in the "non-boundary-layer" flow at the FPJ inlet is $\pm 0.25\%$ of the bulk flow velocity and the r.m.s. turbulence intensity is approximately 1.7%. The boundary-layer thickness of the flow at the inlet is less than 0.75 mm.

Laser Doppler Anemometry

The experiments were performed at the Division of Mechanical Engineering, University of Wales, Cardiff. Measurements of the internal FPJ velocity field were obtained with a 2-colour, frequency-shifted LDA system and a 5-Watt Argon-ion laser. Only the green-beam pair (514.5 nm) was used, and so only the

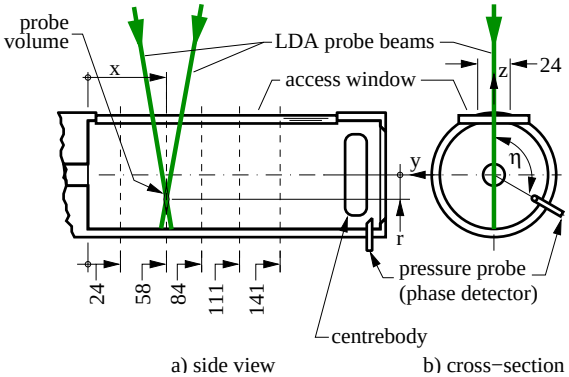

Figure 4: LDA measurement locations; - - - - - - measurement "plane"; $\eta = 120°$.

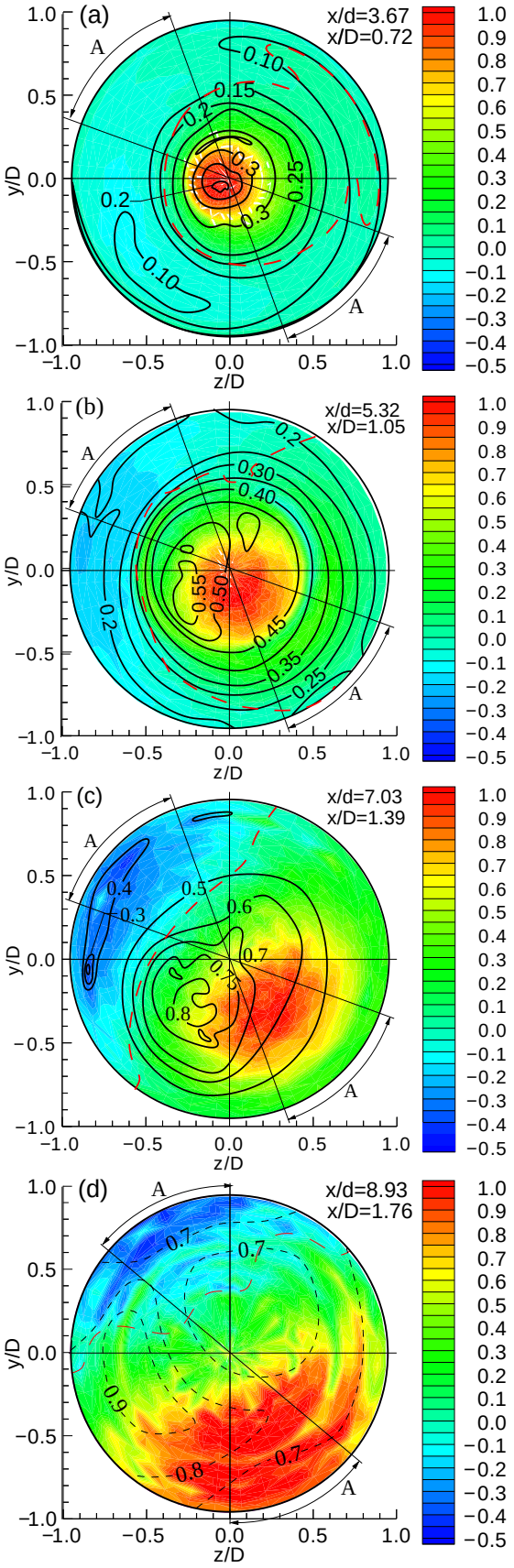

Figure 5: Colourmaps of the phase-averaged mean velocity and contours of phase-averaged r.m.s. velocity fluctuations. Data is non-dimensionalised using the maximum velocity, $U_{x,max}$. $Re_d = 84,500$. The thick (red) dashed lines divide regions of forward and reversed flow.

axial component of velocity was measured.

The LDA optical head has a focal length of 310 mm and a beam separation of 64 mm, giving a green-beam probe volume with a waist diameter of 0.17 mm and a length of 1.65 mm. It was mounted on a Dantec 57G15 three-axis traverse which has a position accuracy of ± 0.05 mm in all three directions.

Phase Averaging Technique

Phase averaging of a precessing-jet flow requires a reference probe which can identify the start time and end time of each 360-degree precession cycle. When the limits of each cycle are identified, the cycle is divided into a number of phase segments, and the corresponding velocity data is accumulated into the phase segments to produce the "ensemble sums". Dividing the array of ensemble sums by the number of precession cycles gives the phase averaged velocity field. In effect, phase averaging generates an average instantaneous flow field.

In the phase averages of Figure 5, phase angle is calculated by assuming that the phase speed (i.e. precession frequency) does not change during a precession cycle. The effect of phase-speed variations is to reduce the measured amplitude of peaks and troughs in the phase-averaged mean flow speed and to increase the measured r.m.s. velocity fluctuations, especially in regions of mean shear flow.

The reference probe for phase averaging was a 3 mm diameter tube with an open end bevelled at 45°. The probe was located midway between the centrebody and the lip of the nozzle, and it was inserted, with its bevelled end facing upstream and protruding 10 mm into the flow. A pressure transducer with a sensitivity of 500 Pa/Volt and a frequency-response time of 1ms was connected to the probe with 300 mm of PVC tube. The result is a signal which represents the variation in total pressure associated with the impact of the precessing-jet flow on the probe. The signal from the pressure transducer was low pass filtered at 10Hz by a 6-pole Butterworth filter and converted to a trigger by a Cathode Ray Oscilloscope (CRO). At each maximum in the filtered signal, the CRO sent a TTL trigger to the LDA signal processor where it was stored as a false LDA signal. The precession frequency, f_p, was about 7.5 Hz.

Experimental Procedure

All the phase averaging measurements were run at an inlet Reynolds number of 84,500 and a bulk inlet velocity, $U_i = 78.7$ m/s. Measurements were obtained along a radius at each of five distances from the FPJ inlet plane (Figure 4). There were 20 measurement positions along each radius, with a radial step size of 2 mm. An average of 14,800 velocity samples and an average of 700 precession cycles were recorded at each LDA measurement position.

The LDA data were processed with Burstware version 3.21 and a collection of small BASIC programs. The phase averaging program divided the 360-degree precession cycle into 36 phase segments.

Phase-averaged velocity field

The colourmaps of phase-averaged mean velocity in Figure 5 are consistent with the results of flow visualisation studies [8] which have identified an asymmetric reattaching jet in the FPJ chamber. Near the inlet ($x/d = 3.67$), the *inlet* flow is axisymmetric. Sideways deflection of the jet is clearly visible further downstream (at $x/d = 5.32$ and $x/d = 7.03$) and, closer to the centrebody, ($x/d = 8.93$) the flow is attached to the wall of the chamber.

Figure 6 compares the non-dimensional centreline velocity of the FPJ inlet flow with the Crow and Champagne [2] data for an unconfined turbulent jet at $Re_d = 83,000$. For the FPJ inlet flow, we define the phase-averaged "centreline" velocity, $U_{\text{jet,cl}}$, as the maximum velocity in the measurement plane rather than the value measured at the axis of the chamber. For the unconfined-jet data, where there is no co-flow or counter-flow ($U_c = 0$), the length of the potential core region is about $6d$ and the slope, $m = -1.07$, in the region $x/d > 9$ indicates a linear spreading

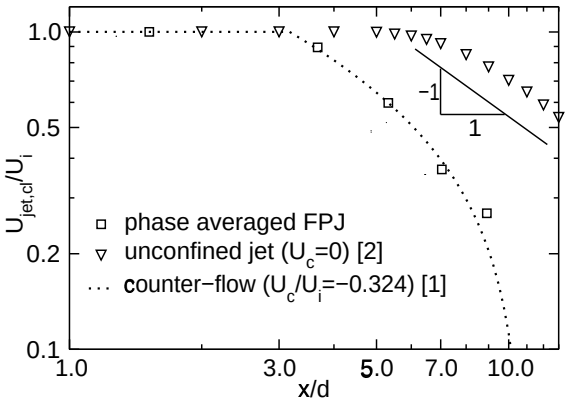

Figure 6: Maximum non-dimensional mean velocity, $U_{\text{jet,cl}}/U_i$, at each phase-averaged cross-section of the FPJ velocity field. U_i = time-averaged velocity at inlet. U_c = co-flow or counter-flow velocity. Note the log-log axes and data from references [1] & [2]. $Re_d = 84,500$.

rate. In contrast, the potential core of the flow from the FPJ inlet orifice has a length of only $3.5d$, and a decay-rate slope of -1.5 for the phase-averaged velocity indicates a non-linear spreading rate.

The large decay rate in Figure 6 implies that the spreading rate of the jet should be larger than for an unconfined jet. This is confirmed in Figure 7 which shows radial distributions of velocity for an unconfined jet and phase-averaged velocity distributions for the FPJ.

Volume flow rate

Study of the volume flow rate at each measurement plane in the chamber offers an explanation for the high spreading angle and high velocity decay rates of the inlet flow. Volume flow rate is proportional to mass flow rate because the flow is isothermal and Mach number is low. The initial calculation of non-dimensional flow rate, Q/Q_i, from the mean velocity data was performed as a consistency check. This is plotted in Figure 8 as a sequence of crosses ($\times$). Rather than the constant value $Q/Q_i = 1$ required by continuity, Q/Q_i increases with distance from the FPJ inlet plane to $Q/Q_i \approx 2$ at $x/d = 8.93$. The most probable sources of error are a lack seeding in the external flow field and LDA sampling-rate bias. The velocity of the reverse induced air flow (Figure 1) is therefore not measured until it has been well-mixed with the seeded jet flow. Loss of signal due to

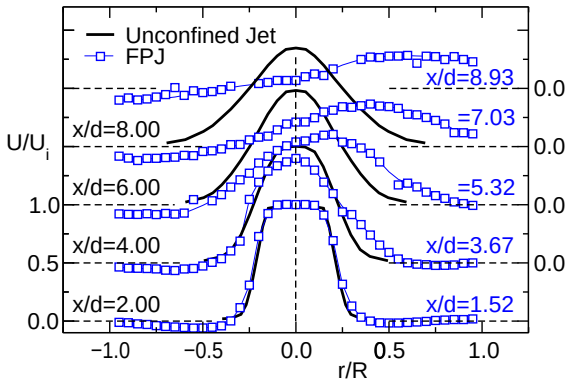

Figure 7: Radial distributions of the phase-averaged axial velocity component for FPJ inlet flow and mean velocity in an unconfined jet [2]. For each axial position the coordinate system is progressively shifted by $U/U_i = +0.5$. The distributions of phase-averaged velocity are obtained by averaging over the phase-angle arcs "A-A" in Figure 5. $Re_d = 84,500$ for the FPJ.

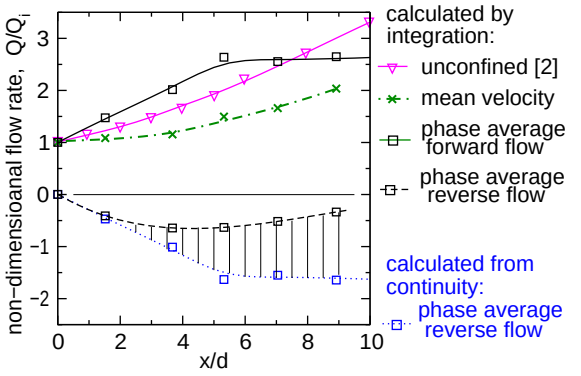

Figure 8: Non-dimensional flow rate in the FPJ nozzle (□, ×), and for an unconfined axisymmetric jet [2] (▽). The hatched region shows the difference between the two methods of calculating reverse flow rate. Q_e is the flow rate at the inlet plane.

condensation on the observation window and the non-uniform seeding prevented removal of the sampling-rate bias.

The phase-averaged mean velocity data provides another method of calculating flow rate. If negative and positive flow speed are integrated separately, it is possible to estimate separate forward and reverse flow rates. These flow rates are plotted in Figure 8 as solid and dashed lines respectively. Error due to non-uniform seeding is expected to make the reverse flow rate integral somewhat less reliable than the forward flow rate integral. A more plausible estimate for reverse flow rate can be obtained from the forward flow rate and continuity:

$$Q_{\text{reverse}} = Q_i - Q_{\text{forward}}. \quad (1)$$

The difference between the two estimates of reverse flow, which is indicated by the hatched region in Figure 8, is similar to the increase in flow rate estimated from the mean velocity data.

In Figure 5, each measurement plane is divided into regions of forward and reverse mean flow by thick dashed lines. The forward flow speed is then averaged over the forward flow area and the reverse flow speed is averaged over the reverse flow area to obtain the flow speed ratios shown in Table 1. These values are based on the flow-rate integrals and so are likely to be accurate to, at most, one significant figure. However, they do indicate the significance of reversed flow in the FPJ nozzle.

Chan and Lam [1] have measured the effect of counter-flow on the centreline velocity of a turbulent jet, and they have produced an advective algebraic model which agrees well with their experimental data. This model also provides an estimate of the effect of counter-flow on the length of the potential-core region. At a counter-flow velocity ratio of $U_c/U_i = 0.324$, which is similar in magnitude to the values in Table 1, the Chan and Lam model produces a centreline-velocity distribution very close to the phase-averaged decay in Figure 6. The length of the potential-core region given by the model, $3.2d$, is also close to the value obtained from the phase-averaged FPJ data.

The flow in the FPJ nozzle is rather different from the flow produced by an unconfined jet in counterflow because, at the very least, the reverse flow is not uniform and the forward flow becomes attached to the wall of the chamber. Nevertheless, the agreement between the Chan and Lam results and the phase-averaged velocity decay in Figure 6 suggests that induced reverse flow has a significant effect on the spreading rate and decay rate of the FPJ inlet flow.

x/d	1.52	3.67	5.32	7.03	8.93
$\frac{U_{\text{reverse}}}{U_{\text{forward}}}$	-0.16	-0.23	-0.37	-0.43	-0.37

Table 1: Estimates of the average reverse flow speed (U_{reverse}) as a fraction of average forward flow speed (U_{forward}). These velocity ratios are determined from the flow rates and areas obtained by integration of the phase-averaged velocity field.

Conclusion

Phase-averaged measurements of the axial velocity component in an FPJ nozzle show that the jet flow from the inlet plane spreads and decays much more rapidly than an unconfined jet. Reasoning based on continuity and estimates of the flow-rate distribution along the nozzle suggest that, in the vicinity of reattachment, the speed of reverse induced flow is about 30% of the forward jet flow speed. Comparison with the experimental data and with the analytical model of Chan and Lam [1] suggests that the reverse flow has a similar effect to that of a counterflow, and is largely responsible for the high spreading angle and high decay rate of the reattaching FPJ inlet flow.

Acknowledgements

Funds from an ARC IREX grant allowed the first author to make the LDA measurements at the University of Wales, Cardiff. He most sincerely thanks the staff and postgraduate students of the university for their help with the experiments.

References

[1] C. H. C. Chan and K. M. Lam. Centreline velocity decay of a circular jet in a counterflowing stream. *Physics of Fluids*, 10(3):637–644, March 1998.

[2] S. C. Crow and F. H. Champagne. Orderly structures in jet turbulence. *Journal of Fluid Mechanics*, 48:547–591, 1971.

[3] C. Manias, A. Balendra, and D. Retallack. New combustion technology for lime production. *World Cement*, December 1996.

[4] C. G. Manias and G. J. Nathan. Low NO_x clinker production. *World Cement*, May 1994.

[5] R. D. Mehta. The design of wide angle diffusers. I. C. Aero Report 76-03, Imperial College of Science and Technology - Department of Aeronautics, June 1976.

[6] J. Mi, G. J. Nathan, and S. J. Hill. Frequency characteristics of a self-excited precessing jet nozzle. In E. Cui, editor, *Proceedings of the Eighth Asian Congress of Fluid Mechanics*, pages 755–758, Shenzhen, China, December 1999. Asian Fluid Mechanics Comittee, International Academic Publishers.

[7] G. J. Nathan. *The enhanced mixing burner*. PhD thesis, Department of Mechanical Engineering, University of Adelaide, Australia, 1988.

[8] G. J. Nathan, S. J. Hill, and R. E. Luxton. An axisymmetric "fluidic" nozzle to generate jet precession. *Journal of Fluid Mechanics*, 370:347–380, 1998.

[9] G. J. R. Newbold, G. J. Nathan, and R. E. Luxton. Large-scale dynamics of an unconfined precessing jet flame. *Combustion Science and Technology*, 126:71–95, 1997.

[10] G. J. R. Newbold, G. J. Nathan, D. S. Nobes, and S. R. Turns. Measurement and prediction of NO_x emissions from unconfined propane flames from turbulent-jet, bluff-body, swirl and precessing burners. *Proceedings of the 28th Int. Symp. on Combustion - the Combustion Institute*, 28:481–487, 2000.

[11] D. S. Nobes. *The generation of large-scale structures by jet precession.* PhD thesis, Department of Mechanical Engineering, University of Adelaide, Australia, 1997.

[12] G. M. Schneider. *Structures and turbulence characteristics in a precessing jet flow*. PhD thesis, Department of Mechanical Engineering, University of Adelaide, Australia, 1996.